https://doi.org/10.1016/j.envpol.2022.119778

Secondary organic aerosol formation at an urban background site on the coastline of South China: precursors and aging processes

Dawen Yao, Hai Guo*, Xiaopu Lyu, Haoxian Lu, Yunxi Huo

Air Quality Studies, Department of Civil and Environmental Engineering, The Hong Kong Polytechnic University, Hong Kong, China

* Correspondence to Hai Guo (ceguohai@polyu.edu.hk)

Abstract: Understanding the formation mechanisms of secondary organic aerosols (SOA) is an arduous task in atmospheric chemistry. In November 2018, a sampling campaign was conducted at an urban background site in Hong Kong for characterization of secondary air pollution. A high-resolution time-of-flight aerosol mass spectrometer was used to monitor the compositions of non-refractory submicron particulate matters (NR-PM_1), and multiple online instruments provided us with comprehensive auxiliary data. Organic aerosol (OA) constituted the largest fraction (43.8%) of NR-PM_1, and 86.5% of the organics was contributed by the oxygenated OA (OOA, secondary components). Formation mechanisms of a dominant and more variable component of the less-oxidized OOA (labelled as LO-OOA1 in this study) and the more-oxidized OOA (MO-OOA) were explored. Based on the multilinear regression with molecular markers of OA (e.g., hydroxybenzonic acids and 2,3-dihydroxy-4-oxopentanoic acid), we presumed that anthropogenic organic compounds, especially aromatics, were the most likely precursors of LO-OOA1. MO-OOA correlated well with odd oxygen (O_x), and its concentration responded positively to the increase of liquid water content (LWC) in NR-PM_1, indicating that the formation of MO-OOA involved photochemical oxidation and aqueous processes. It exhibited the best correlation with malic acid which can be formed through the oxidation of various precursors. Moreover, it was plausible that LO-OOA1 was further oxidized to MO-OOA through aqueous processes, as indicated by the consistent diurnal variations of MO-OOA to LO-OOA1 ratio and LWC. This study highlights the important roles of anthropogenic emissions and aqueous processes in SOA formation in coastal areas downwind of cities.

Keywords: Secondary organic aerosols; Organic aerosol markers; Aqueous processes; Photochemical oxidation; Anthropogenic emissions

1. Introduction

Airborne particulate matters (PM) have a proven impact on climate (Seinfeld and Pandis, 2008; Jacob and Winner, 2009) and air quality (Huang et al., 2014; Elser et al., 2016). Organic aerosols (OA), comprising a broad spectrum of compounds with different volatilities and properties (De Gouw and Jimenez, 2009; Zhang et al., 2011), account for substantial mass fractions (20−90%) of PM (Kanakidou et al., 2005; Jimenez et al., 2009). While some OA compounds can be directly emitted from diverse anthropogenic and natural sources, termed as

primary OA (POA), the secondary organic aerosols (SOA) are formed through chemical evolutions of organic compounds (Donahue et al., 2006; Kroll and Seinfeld, 2008; Li et al., 2016). SOA formation is influenced by a number of factors, such as atmospheric oxidation capacity, precursor, reaction media, and meteorology (Hu et al., 2017; Xu et al., 2017; Brege et al., 2018; Paglione et al., 2020).

In China, Xu et al. (2017) studied the roles of photochemical oxidation and aqueous processes in altering the compositions and oxidation degrees of oxygenated OA (OOA) in Beijing. It was indicated that aqueous processes dominated the formation of the more oxidized OOA (MO-OOA). The consistent findings were reported by Xiao et al. (2021), who examined the joint effects of relative humidity (RH) and odd oxygen (O_x) on SOA formation. Huang et al. (2020) inspected the dependences of OOA components on O_x and liquid water content (LWC) at a background site of the Yangtze River Delta region in summer. They found that the formation of OOA at higher oxidation state was mainly driven by photochemical oxidation. Such discrepancies indicated that SOA formation mechanisms might not always be consistent. Aerosol Mass Spectrometer (AMS) measures concentrations and compositions of non-refractory submicron particulate matters (NR-PM_1) at extraordinary time resolutions, i.e., a few seconds to minutes (Jayne et al., 2000; Canagaratna et al., 2007). It has been extensively used to study the evolution of OA in the atmosphere (DeCarlo et al., 2010; He et al., 2011; Kim et al., 2017). However, based on AMS data only, it is hard to determine the precursors and specific formation pathways of SOA, because AMS fails to provide any molecular information. With the aid of other unambiguous measurements, the interpretability of AMS data can be enhanced. For example, Xu et al. (2015) determined the isoprene-derived SOA based on the correlation with 2-methyltetrols and showed the mediation effect of sulfate on this component in the southeastern United States.

Hong Kong, an Asian metropolis in South China and adjoining the fast-developing Pearl River Delta (PRD) region in mainland China, has undergone PM pollution for decades (So et al., 2007; Lin et al., 2018). In addition to local sources, such as vehicular and cooking emissions (Lee et al., 2015; Yao et al., 2021), regional and even superregional transport can aggravate PM pollution in Hong Kong, especially in cool seasons (Wang et al., 2017; Lyu et al., 2020). The compositions, sources and evolutions of OA in Hong Kong have been extensively studied (Li et al., 2013; Hu and Yu, 2013). Vehicular and cooking emissions made significant contributions (44.6% - 65.0%) to OA at urban roadside sites (Lee et al., 2015; Yao et al, 2021). Li et al. (2013) indicated that aqueous processes were likely responsible for the high degree of oxygenation for OA at an urban background site during the spring foggy period. Qin et al. (2016) analyzed the evolutions of OA during PM episodes at the same site and identified the roles of photochemical oxidation and aqueous processes in SOA formation. With the filter-based measurement data, Hu and Yu (2013) deduced aqueous formation of malic acid through the oxidation of multiple precursors. Most of the previous studies (e.g., Li et al., 2013; Qin et al., 2016) intended to understand aqueous chemistry were conducted in spring, because Hong Kong has the highest relative humidity and cloud amount from March to June. However, this city experiences most serious photochemical pollution in autumn when the ozone levels were significantly higher than those in many inland cities (Liu et al., 2021). Besides, transboundary transport brought aged air masses from China mainland to Hong Kong in cool seasons.

Therefore, SOA formation in autumn merits investigation. Moreover, the AMS-based studies failed to identify the precursors of SOA, and low time resolution was an inherent defect of filter-based studies.

In this work, a High Resolution-Time of flight-AMS (HR-Tof-AMS) was used for real-time measurement of NR-PM_1 compositions at an urban background site, which was also a coastal site, in Hong Kong. The temporal variations of NR-PM_1 components and the sources of OA are discussed. We focus on the formation mechanisms of two dominant OOA components. The study also sheds light on the potential precursors of OOA. The findings enhance understanding on the chemical evolutions of OA in urban background atmosphere and provide scientific basis for controlling OA pollution that is increasingly concerned.

2. Methodolgy

2.1. Sampling site

A sampling campaign was carried out in November 2018 at an air quality monitoring station (Hok Tsui, HT) managed by the Hong Kong Environmental Protection Department (HKEPD). The theme of this field campaign was to observe photochemical air pollution in subtropical Hong Kong. The site (22.209° N, 114.253° E) was located at the southeast tip of Hong Kong, facing South China Sea to the east and south (Figure 1). The local emissions were sparse despite a small village nearby. East-northeast winds prevailed at the site in autumn. Therefore, air pollutants in Hong Kong urban areas and the adjoining Pearl River Delta (PRD) can be transported to the site. For this reason, HT has been regarded as an urban background site in South China (Zhang et al., 2012; Wang et al., 2019; Lyu et al., 2020). The sampling inlet was ~1 m above the roof of a one-story building (~3 m), and a PM_1 cyclone (URG-2000-30EHB) was used to remove the large particles from the air drawn into the instruments (Lyu et al., 2020). In addition to the HR-Tof-AMS, many other instruments were deployed at the site, which provide auxiliary data for this study.

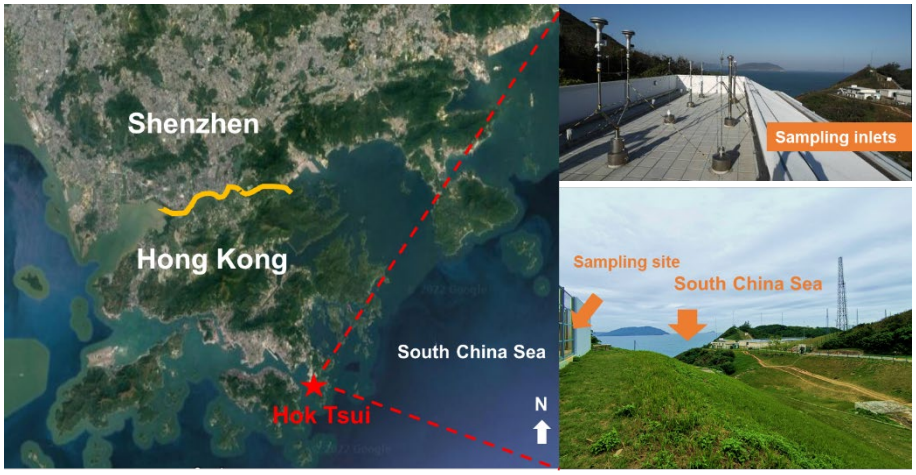

Figure 1. Location of the sampling site (star in left panel) and real scene of sampling inlets and environment (right panels). Boarder line between Shenzhen and Hong Kong is highlighted in yellow.

2.2. Measurement techniques

2.2.1. HR-Tof-AMS measurement and data processing

The NR-PM_1 compositions, including total organics, sulfate, nitrate, ammonium and chloride, were measured using an Aerodyne HR-Tof-AMS (Jayne et al., 2000; DeCarlo et al., 2006). The instrument was operated between two ions optical modes alternatively every 2 min., *i.e.*, V-mode with higher sensitivity and W-mode with higher mass resolution. A complete V mode cycle consisted of 6 sub-cycles, and every sub-cycle of 20s was divided into 10s of mass spectrum (MS) mode (5s chopper-open and 5s chopper-closed) and 10s of particle time-of-flight (PToF) mode. As such, the size distributions were measured for the NR-PM_1 components, where the sizes were in unit of mass-weighted aerodynamic diameter. In each W mode, data were acquired in 12 sub-cycles of 10 s MS mode (5s chopper-open and 5s chopper-closed). The ions detected in W-mode with high mass resolution (~5000–6000) allow us to determine the elemental compositions of organics (DeCarlo et al., 2006; Aiken et al., 2008; Sun et al., 2011), which therefore are used in source apportionment.

The raw data were processed in accordance with the methods described in previous studies, using the standard Tof-AMS Analysis Toolkit 1.59D and Tof-AMS HR Analysis 1.19D (Jimenez et al., 2003; DeCarlo et al., 2006). The default relative ionization efficiency (RIE) of 1.2, 1.1, 1.3 and 1.4 were adopted for sulfate, nitrate, chloride and organics, respectively (Canagaratna et al., 2007). The RIE of 4.0 was assigned to ammonium, based on the regular weekly ionization efficiency calibrations. The m/z 30 and m/z 46 were calibrated for ionization efficiency (IE) using pure ammonium nitrate particles with a size of 350 nm. An air flow calibrator (Drycal DC-Lite) was used to calibrate the sampling flow rate. Particle velocity was calibrated using Nanosphere PSL particles (Duke Scientific, Palo 120 Alto, CA, USA) with sizes of 50, 100, 200, 300, 400, 500 and 600 nm. By comparing the AMS NR-PM_1 with PM_1 minus black carbon measured by the HKEPD, we determined the collection efficiency (CE) as 0.73, which was introduced in our previous study (Lyu et al., 2020). The CE factor was applied to all the measured PM_1 components. Particle-free ambient air was sampled through an inline HEPA-filter for ~60 minutes every 2-3 days to obtain the background concentrations, which were subtracted from the ambient data and were used to calculate the method detection limits (MDLs). The MDLs were determined to be 0.211, 0.022, 0.020, 0.013, and 0.013 μg/m^3 for organics, sulfate, nitrate, ammonium and chloride, respectively. The CO_2^+ signal was corrected for the real-time contributions from CO_2 gas. The elemental ratios of oxygen to carbon (O:C) and hydrogen to carbon (H:C) were determined following the method updated by Canagaratna et al. (2015).

The high resolution MS data of organics were analyzed using the PMF2 algorithm in robust mode (Paatero and Tapper, 1994) with the PMF Evaluation Toolkit (PET ver 2.05) (Ulbrich et al., 2009). A minimum error value was applied to the error matrix, and each ion was assessed

and treated according to its signal-to-noise ratio (SNR). Ions with an average SNR of less than 0.2 were removed, and those with a SNR between 0.2 and 2 were down-weighted by increasing their errors by a factor of 2. Furthermore, the errors for ions related to m/z 44 (i.e., CO_2^+, CO^+, H_2O^+, HO^+, and O^+) were also increased by 2-3 folds to reflect the influences of CO_2^+. Isotopes were removed from the matrices, because their signals were scaled to their parent ions rather than being measured directly.

2.2.2 Other measurements

Criteria air pollutants, nitric oxide (NO) and meteorological parameters were monitored by the HKEPD. Details about the measurements can be found in previous studies (Lyu et al., 2020; Tan et al., 2021). All the instruments were regularly calibrated following the quality control and quality assurance (QC/QA) protocol identical to that adopted by the US air quality monitoring program (Lyu et al., 2020). The molecular makers of OA used in this study were measured by an online Thermal-desorption Aerosol Gas-chromatograph coupled with time-of-flight mass spectrometry (TAG). Details about the measurement and data processing have been provided in Lyu et al. (2020). Volatile organic compounds (VOCs) were measured using a proton transfer reaction mass spectrometry (Tan et al., 2021). During the sampling period, the average ambient temperature, relative humidity and wind speed were 22.5 ± 0.1 °C (mean ± 95 confidence interval, the same elsewhere), 79.9 ± 0.8 % and 4.6 ± 0.1 m/s, respectively. The dominant winds were easterly and northeasterly. All the data are converted into hourly averages for analysis, except for TAG data. In this campaign, the TAG was operated at the resolution of 1.5 h per sample. Wherever TAG data are used, the other data with higher time resolutions are averaged in the TAG sampling intervals for matching purpose.

2.3. Estimation of liquid water content

The LWC in PM_1 was calculated using the Extended AIM Aerosol Thermodynamics (E-AIM) Model, which was developed for characterization of the gas/liquid/solid partitioning in aerosol systems (http://www.aim.env.uea.ac.uk /aim/aim.php). In this study, the E-AIM IV (Wexler and Clegg, 2002; Friese and Ebel, 2010) was used, where the inorganic compositions of PM_1 measured by HR-Tof-AMS, temperature and relative humidity were input. Figure 2 shows the time series and diurnal patterns of the calculated LWC, temperature and relative humidity. The average LWC during this sampling period was 10.4 ± 0.6 μg/m^3, comparable to the previously reported level of 12.8 μg/m^3 in autumn in Hong Kong (Li et al., 2013; Qin et al., 2016). While the variation of LWC resembled the pattern of relative humidity, the correlation between them was moderate (r^2 = 0.52), mainly due to the influence of water soluble ions.

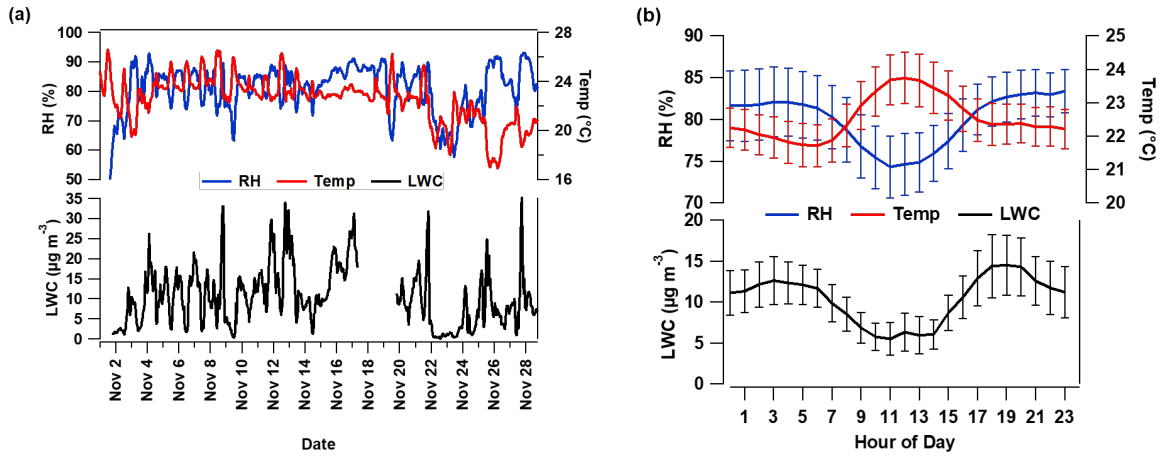

183

184 Figure 2. Time series (a) and average diurnal variations (b) of the calculated LWC, temperature
185 (temp) and relative humidity (RH) during the sampling period. Missing data of LWC are due
186 to unavailability of inorganic compositions in PM_1 during AMS maintenance. Error bars in (b)
187 represent 95% confidence intervals (CIs), and the same elsewhere.

188

189 **3. Results and Discussion**

190 **3.1. General features**

191 Figure 3 shows the time series of the NR-PM_1 components and the average compositions of
192 NR-PM_1. The hourly concentration of NR-PM_1 ranged from 3.0 to 32.4 μg/m^3, with a mean of
193 13.5 ± 0.4 μg/m^3. The total concentration of organics was 6.0 ± 0.2 μg/m^3, varying between
194 1.1 μg/m^3 and 16.0 μg/m^3. The fraction of total organics (43.8 ± 0.7 %) was followed by that
195 of sulfate (35.8 ± 0.7 %), ammonium (14.4 ± 0.2 %), nitrate (5.4 ± 0.2 %) and chloride (0.7 ±
196 0.02 %), whose concentration was 4.7 ± 0.1, 1.9 ± 0.1, 0.8 ± 0.05 and 0.08 ± 0.01 μg/m^3,
197 respectively. Mainly due to the lower emissions of POA at HT, the organics fraction was lower
198 than that (>50%) at the urban roadside sites in Hong Kong (Lee et al., 2015; Yao et al., 2021).
199 However, it was markedly higher than that (31%) at another background site (HKUST) ~14
200 km to the north of HT (Li et al., 2015). This was attributable to the lower concentrations of
201 other PM_1 components at HT, because the concentrations of were organics comparable (13.5
202 μg/m^3 at HT *vs.* 15.9 μg/m^3 at HKUST). In particular, the average concentration of sulfate was
203 7.4 μg/m^3 at HKUST, 57.4% higher than our observation at HT. Note that the HKUST
204 measurement conducted in 2011 witnessed much higher mixing ratio of sulfur dioxide (3.4
205 ppbv), compared to the 1.2 ppbv observed at HT in 2018. Therefore, in this study, the lower
206 level of sulfate was likely a result of the declining precursor.

207 Despite the potential concentration reduction over time, the mass fraction of sulfate at HT was
208 significantly higher than that (23.1 ± 0.4 %) measured at an urban roadside site in recent years
209 (Yao et al., 2021). On one hand, regional transport might be partially responsible for the high
210 levels of sulfate at this urban background site. On the other hand, the relatively high levels of
211 relatively humidity (72.7 %) and atmospheric oxidation capacity (reflected by O_x of 49.8 ppbv)

in the coastal area could facilitate aqueous formation of sulfate (Li et al., 2015). The aqueous chemistry is confirmed in analysis of SOA formation mechanisms (section 3.3).

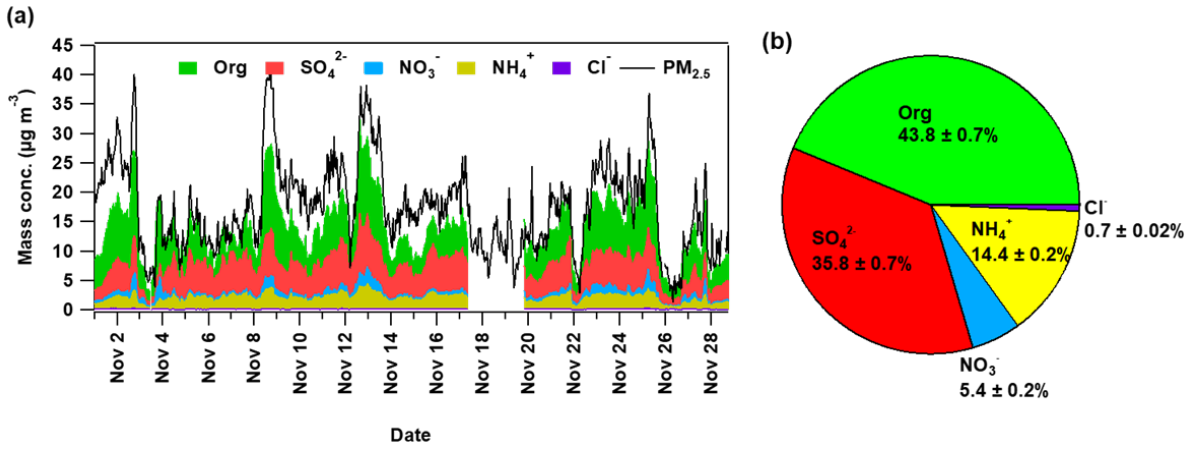

Figure 3. Time series of NR-PM_1 components and $PM_{2.5}$ (a); and average compositions of NR-PM_1 at HT (b). Org: total organics, SO_4^{2-}: sulfate, NO_3^-: nitrate, NH_4^+: ammonium, Cl^-: chloride. Missing data of NR-PM_1 components are due to instrument maintenance.

The diurnal variations of NR-PM_1 and the components therein are shown in Figure S1. Higher levels of NR-PM_1 were observed in daytime, indicating intensive photochemical formation of secondary aerosols, which overwhelmed the effect of higher boundary layer height. The total organics showed a broad peak from 11:00 to 20:00, consistent with the pattern of NR-PM_1. It implied that SOA constituted a significant fraction of the total organics and modulated the diurnal variation of NR-PM_1. Differently, an obvious trough was identified for the diurnal pattern of nitrate during 11:00-14:00, which could be caused by the enhanced evaporation in this period when the temperature was high (Figure 2). The diurnal pattern of sulfate differed from that of the total organics mainly in the afternoon, when the former continued to increase while the latter was relatively stable on the plateau. Due to the increase of LWC from noon to early evening (Figure 2), the rise in sulfate concentration in the afternoon might be attributable to aqueous formation. The relatively stable concentration of total organics between 11:00 and 20:00 did not necessarily indicate no chemical evolution. Instead, we speculate a potential transformation of the organics towards higher oxidation states (section 3.3), which might not lead to notable change in the total concentration of organics. Ammonium followed the pattern of sulfate, because of the charge balance and dominance of sulfate in anions. Lastly, the diurnal variation of chloride with lower concentrations in daytime was shaped by the development of boundary layer and temperature-dependent partitioning between gas and particle phases.

3.2. Source apportionment of OA

To further study the organics in NR-PM_1, it is necessary to break it down to OA components of different characteristics. Hence, source apportionment was applied to the organics. The most appropriate results were determined based on the principles described in previous studies

(Ulbrich et al., 2009; Zhang et al., 2011), taking into account the mathematical criterions and physical meanings of the factors. The number of factors from 2 to 7 was tested, and the corresponding Q/Q_{exp} values were calculated (Figure S2). For the solution with each number of factors, the rotational ambiguity was tested with the FPEAK ranging from -2 to 2 in steps of 0.2. According to the variation of Q/Q_{exp} value with the number of factors and the interpretability of the mass spectra, a 4-factor solution was finally accepted. They included a factor of hydrocarbon-like OA (HOA, a type of POA) and three factors representing OOA (SOA).

The mass spectra of the four identified factors are shown in Figure 4(a). HOA is mainly associated with primary emissions of fossil fuel combustion (Zhang et al., 2005; Lanz et al., 2008). Here, the main ions in the HOA factor were the alkyl fragments ($C_nH_{2n+1}^+$ and $C_nH_{2n-1}^+$), such as m/z 41 ($C_3H_5^+$), 43 ($C_3H_7^+$), 55 ($C_4H_7^+$) and 57 ($C_4H_9^+$), in line with the HOA spectra reported before (Ng et al., 2011; Sun et al., 2011). The HOA factor had the highest H:C ratio (1.84) and conversely the lowest O:C ratio (0.24). The O:C ratio was at the upper end of the range for HOA, i.e., 0.05–0.25 (Canagaratna et al., 2015), which was also higher than those at the other sites in Hong Kong (Lee et al., 2015; Yao et al., 2021). This might be due to the fact that air masses at this background site were more aged. Therefore, the contribution of HOA might be somewhat overestimated. The OOA factors had lower loadings of alkyl fragments and higher loadings of oxygenated species than the HOA factor. Consistent with previous studies (Lanz et al., 2007; Ulbrich et al., 2009; Sun et al., 2011), the mass spectra of the OOAs were characterized by dominant fractions of m/z 44 (mainly CO_2^+), an ion tracer of SOA. Two out of the three OOA factors were less oxidized with the O:C ratio of 0.72 (0.76) and H:C ratio of 1.47 (1.46), referred to as LO-OOA1 (LO-OOA2). The other OOA factor was defined as more oxidized OOA (MO-OOA), because of the much higher O:C ratio (1.12) and lower H:C ratio (1.15).

Time series of the four identified OA factors are presented in Figure S3. HOA and LO-OOA1 somewhat resembled each other in the variation, differing from LO-OOA2 which was relatively stable except for the co-enhancements in a few time slots. The diurnal variations were significant for MO-OOA on most days. Further, the relationships between the OA factors and ion tracers were examined (Figure S4). As expected, HOA correlated fairly well with POA tracers ($C_3H_7^+$, $C_4H_9^+$ and $C_6H_{10}O^+$), and the relationship with CO_2^+ was much weaker (r^2 = 0.22). $C_6H_{10}O^+$ is used to indicate cooking organic aerosol (COA) (Sun et al., 2011; Kim et al., 2017), an important source of OA identified in urban areas of Hong Kong (Lee et al., 2015; Liu et al., 2019). However, COA was not discerned at this site. The good correlation between HOA and $C_6H_{10}O^+$(r^2 = 0.80) suggests that a fraction of COA might be allocated to HOA, due to co-variation of them formed during transport. Interestingly, while LO-OOA1 varied consistently with CO_2^+ (r^2 = 0.75), it also exhibited good correlations with the POA tracers (r^2 = 0.61–0.76). It indicated that LO-OOA1 might represent the earlier generation oxidation products of primary emissions, such as vehicle and cooking emissions. Poorer correlations were identified between LO-OOA2 and all the tracers, however the correlation with CO_2^+ was the best (r^2 = 0.56). MO-OOA, as the most oxidized OA factor, was not related to POA tracers and correlated moderately with CO_2^+ (r^2 =0.37). While biomass burning was suspected as a large contributor to OA at the same site (Lyu et al., 2020), the high contributions were

determined with a reconstruction method based on the concentrations of molecular tracers and were mainly identified in December 2018 when the AMS data was not available. However, it is hard to completely eliminate the interferences of other sources.

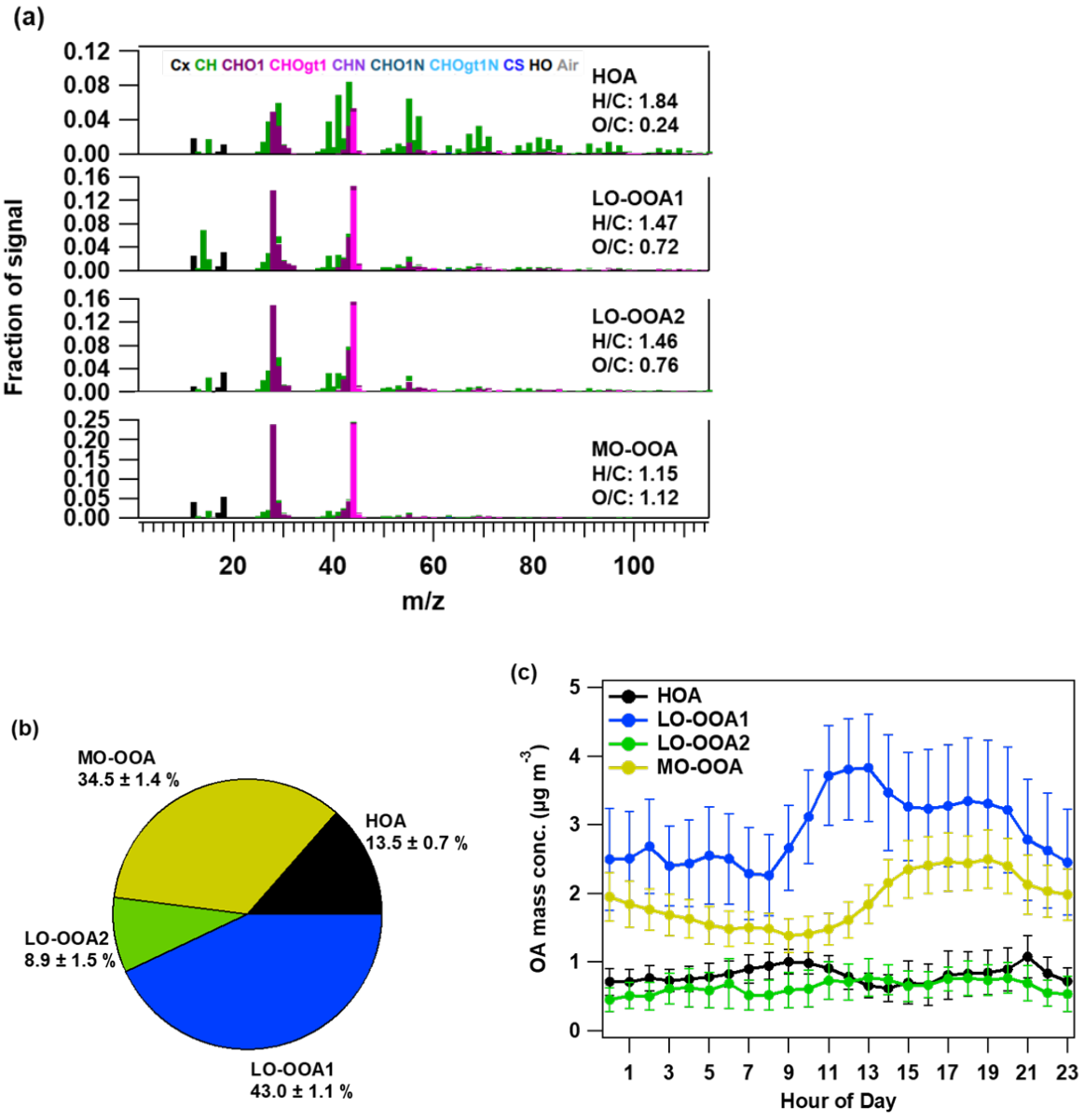

Figure 4. Mass spectra of OA factors resolved from source apportionment (a); Percentage contributions to the total organics of the identified sources (b); and Diurnal patterns of the specific sources (c).

Overall, OOAs dominated the contributions (86.5 ± 0.07 %) to the total organics, while HOA only accounted for 13.5 ± 0.7% (Figure 4b). LO-OOA1 was the largest source of OA with the contribution of 43.0 ± 1.1%. Second to it was MO-OOA, which was responsible for 34.5 ± 1.4% of the total organics. The factor LO-OOA2 made the least and relatively stable contribution (8.9 ± 0.5%) throughout the field campaign, likely representing the background levels of OOA at the site.

Figure 4(c) shows the diurnal variations of OA assigned to the four sources. The HOA got highest concentrations at ~9:00 and ~ 21:00, later than the corresponding peaks of HOA in urban areas (Lee et al., 2015; Yao et al., 2021). Such delay could be due to the transport of emissions from the upwind cities. While the variation of LO-OOA2 was small throughout the day, the significantly higher levels of LO-OOA1 and MO-OOA in the daytime indicated intensive SOA formation involving photochemical processes. The peak of LO-OOA1 appeared at ~13:00, earlier than the broad peak of MO-OOA during 15:00 – 20:00. When the LO-OOA1 decreased between 13:00 and 16:00, the MO-OOA continued to increase. The different patterns were attributable to different formation mechanisms of the two OOA components and potential transformation between them, which are discussed below.

3.3. Formation mechanisms of LO-OOA1 and MO-OOA

The above analyses implied the processes of photochemical and aqueous oxidations in SOA formation. To understand the role of photochemical oxidation, we examined the correlations between OOAs and the odd oxygen O_x ($O_x = O_3 + NO_2$) (Clapp and Jenkin, 2001). As a measure to eliminate the interference of diurnal patterns to the correlation, daily averages are used in the analysis. It was found that MO-OOA responded positively to O_x with a moderate correlation ($r^2 = 0.69$), as shown in Figure 5 (a). As such, the formation of MO-OOA was associated with photochemical oxidation. Furthermore, the high levels of MO-OOA were accompanied by high LWC values, and the diurnal patterns of MO-OOA and LWC resembled each other. The daily average MO-OOA responded positively to LWC, and the correlation was significant ($r^2 = 0.26$, $p < 0.01$), albeit weak (Figure S5). To further reveal the effect of LWC, we plot MO-OOA against LWC at hourly resolution and in 5 LWC intervals (Figure 5(b)). Similarly, weak correlation was identified between the hourly MO-OOA and LWC. The method of averaging variables in a few intervals has been widely adopted in correlation analysis (Marshall et al., 2008), which is capable of reducing the influences of other factors. Obviously, the concentration of MO-OOA increased with the rise in LWC level in the five intervals, and the positive correlation was very significant ($r^2 = 0.96$). As such, it was likely that the MO-OOA formation involved aqueous processes, but it was also subject to other mechanisms, given that LWC expalined small fractions of the hourly and daily variations of MO-OOA. It is noteworthy that the LWC was relatively low in this campaign, which however did not necessarily eliminate aqueous processes. For example, Huang et al. (2020) indicated aqueous formation of MO-OOA in the LWC range of <10 – 40 μg/m^3. Photochemical oxidation and aqueous processes might play roles in different stages of chemical evolution, or they were coupled, e.g., formation of aqueous oxidants through photochemical reactions.

It was indicated that some oxygenated compounds of primary emissions might be assigned to LO-OOA due to similarity in elemental compositions, such as saccharides from biomass burning and fatty acids from cooking (Zhou et al., 2021). However, LO-OOA1 had no correlation with the corresponding molecular tracers (e.g., levoglucosan and oleic acid). Therefore, it was not significantly interfered by either biomass burning or cooking in this study. Instead, it was more likely a representation of earlier generation oxidation products of primary

emissions, as discussed above. Even so, there was nearly no correlation between LO-OOA1 and O_x or LWC (Figure S6), implying that the formation of LO-OOA1 was regulated by other factors, e.g., precursors and/or oxidants other than O_x, and was independent of aqueous processes.

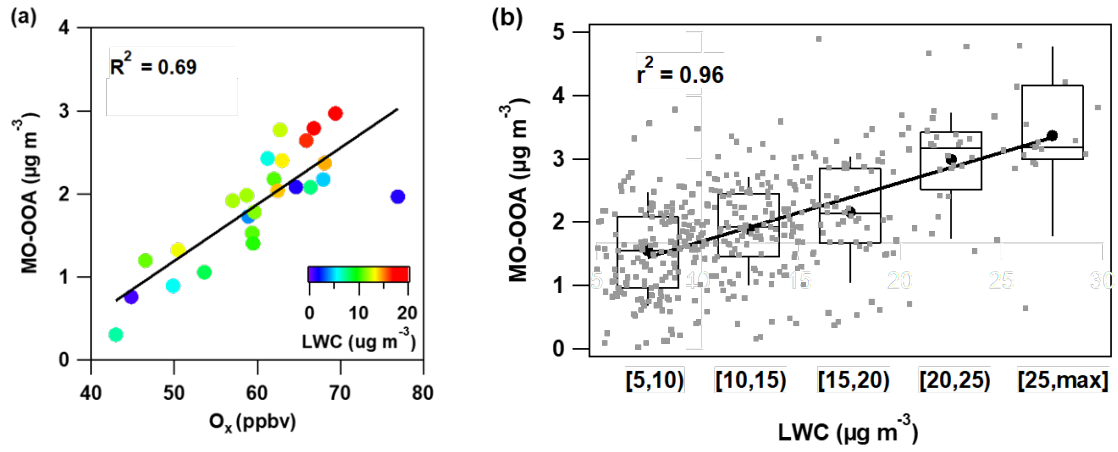

Figure 5. Scatter plot of daily average MO-OOA versus O_x as a function of LWC level (a); Variation of MO–OOA with LWC at hourly resolution (grey dots) and in 5 intervals (boxes) (b).

Further, the potential precursors of OOAs were explored. We examined the diurnal patterns of VOCs and noticed that the peaks of LO-OOA1 and MO-OOA were later than those for toluene and biogenic VOCs (isoprene and monoterpenes), respectively (Figure S7). While further relationship was not found between OOAs and VOCs, we identified moderate to good correlations between OOAs and OA markers that could be formed through oxidation of VOCs. LO-OOA1 exhibited the best correlation with hydroxybenzonic acids (OHBAs) with r^2 of 0.48 (Fugure 6a). Besides, the variations of LO-OOA1 were occasionally synchronized with some other OA markers, such as 2,3-dihydroxy-4-oxopentanoic acid (DHOPA). To identify as many factors accounting for the variations of LO-OOA1 as possible, we performed a series of multilinear regressgions between LO-OOA1 and the OA markers. Through tests, the regression with a highest r^2 of 0.66 and OHBAs, DHOPA and malic acid as the independent variables was determined, as summarized in Table S1. The r^2 of 0.66 suggests that the sources or processes represented by these OA markers explained 66% of the variations of LO-OOA1. OHBAs have been detected in primary emissions of biomass burning and can also be secondarily formed through oxidation of aromarics, e.g., naphthalene and benzonic acid (Wang et al., 2020). Here, due to the poor correlation between OHBAs and levoglucosan (r^2 = 0.06) and higher concentrations of OHBAs in daytime (Figure S8), the OHBAs were most likely secondary products. In addition, DHOPA is a typical tracer of anthropogenic SOA derived from aromatics (Al-Naiema and Stone, 2017). The small and negative coefficient for malic acid implied a potential transformation, which is discussed below. Overall, aromatics were the most likely precursors of LO-OOA1. Due to the relatively low O_3 levels in the morning, hydroxyl-initiated oxidation was a plausible pathway leading to the formation of LO-OOA1, which also explained the poor correlation between LO-OOA1 and O_x.

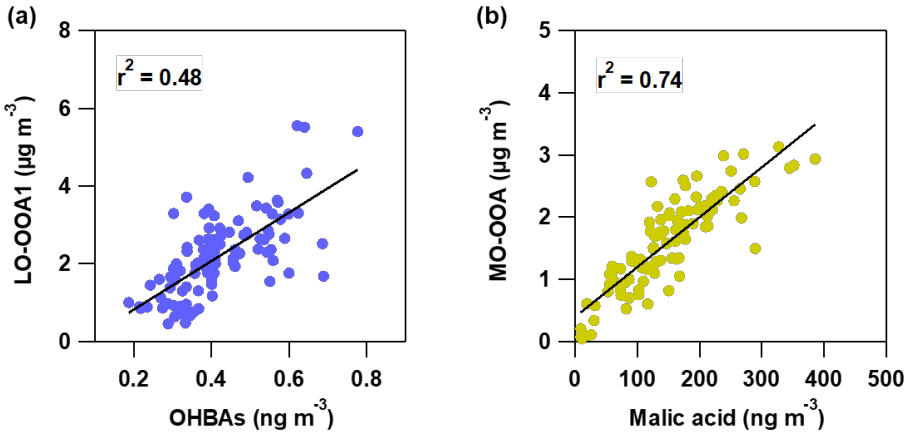

Figure 6. Correlations between OOA and molecular markers of OA: LO-OOA1 vs. OHBA (a); and MO-OOA vs. malic acid (b).

Malic acid was the OA marker that correlated best with MO-OOA (r^2= 0.74), as shown in Figure 6(b). Multilinear regressions with more OA markers as independent variables did not increase the coefficient of determination too much, which therefore were not adopted. According to Lyu et al. (2020), the evidence of biogenic VOCs fuelling malic acid formation was not found in this campaign. Instead, anthropogenic VOCs were suspected as the main precursors of malic acid, due to the moderate correlation between malic acid and DHOPA (Lyu et al., 2020). As a verification, Figure S9 presents the dependences of MO-OOA on the sum of monoterpenes SOA tracers (MT-SOA-T) and the sum of isoprene SOA tracers (Isop-SOA-T) in different air masses. The species included in MT-SOA-T and Isop-SOA-T and classification of air masses were introduced in Lyu et al. (2020). It can be seen that the data points are spread out. While the concentrations of biogenic SOA tracers were higher in continental air, the levels of MO-OOA were lower due likely to the lower O_x. However, the bad correlation ($r^2 < 0.25$) between MO-OOA and MT-SOA-T or Isop-SOA-T in any individual type of air masses suggested that biogenic VOCs might not be the main precursors of MO-OOA.

It is interesting to note that the ratio of MO-OOA/LO-OOA1 showed highly consistent diurnal pattern with that of LWC (Figure 7). In particular, the consistency in the early afternoon when LO-OOA1 decreased and MO-OOA increased most likely indicated that aqueous processes were involved in the transformation of LO-OOA1 to MO-OOA. This partly explained the correlation between MO-OOA and DHOPA (r^2=0.59), as shown in Figure S10. Therefore, like malic acid, MO-OOA might also be the aging product of anthropogenic organics. However, due to the lack of direct evidence and various precursors of malic acid (Wang et al., 2008; Hu and Yu, 2013), we leave the precursors of MO-OOA an open question to be answered in future research. In fact, we found that malic acid correlated fairly well with some biogenic SOA tracers at the same site in another field campaign in 2020 (unpublished data). The discrepancies could be caused by many factors, such as the fewer biogenic SOA tracers detected in 2018, recent emission control of some anthropogenic sources (e.g., ship emissions), and meteorological differences.

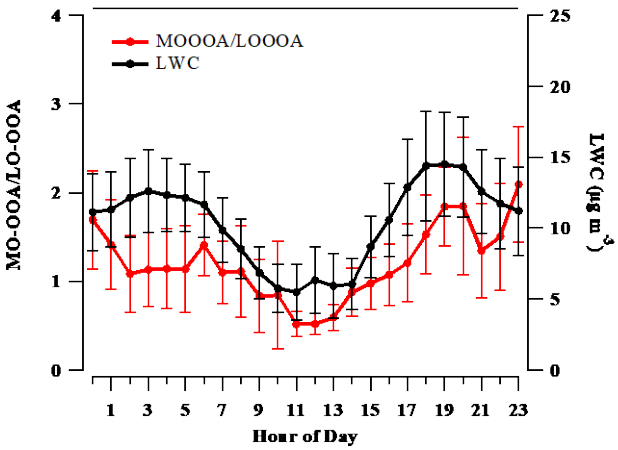

Figure 7. Average diurnal variations of the ratio of MO-OOA/LO-OOA1 and LWC at HT.

4. Conclusions

SOA in the atmosphere is of serious concern for its impacts on air quality, climate and human health. However, the formation mechanisms of SOA in regions significantly affected by human activities have not been fully understood. At an urban background site on the coastline of South China where the SOA chemistry could be complicated by interactions of air pollutants with different sources and origins and changeable meteorology, we discovered high loadings of organics with absolute dominance of SOA in NR-PM_1 in a cool season. The LO-OOA components dominated over MO-OOA and accounted for more than half of the PM_1-bound organics in mass concentration. We proved that one of the LO-OOA components that was more variable and overwhelmed its counterpart in concentration was mainly formed through hydroxyl-initiated oxidation of aromatics. This mainly occurred before noon and seemed not to be limited by O_x and LWC. Subsequently, significant formation of MO-OOA in the afternoon was revealed. While there was no clear conclusion on the precursors of MO-OOA, we proposed the potential transformation from LO-OOA to MO-OOA involving aqueous processes. Photochemical oxidation also modulated MO-OOA formation and brought OA to a higher oxidation state. The photochemical and aqueous processes could be staggered or synergistic. Taking advantages of the other measurements in addition to AMS data, such as molecular OA markers measured by TAG, this study advanced our understanding on the formation mechanisms and precursors of SOA. In particular, the importance of anthropogenic VOCs in contributing to SOA formation in coastal air was highlighted, where the high relative humidity and atmospheric oxidation capacity also played significant roles in OA aging. Similar conditions are common in marginal seas and estuaries close to cities, hence more in-depth studies on SOA formation in representative regions are necessary.

Acknowledgements

This study was supported by the Research Grants Council of the Hong Kong Special Administrative Region via the NSFC/RGC Joint Research Scheme (N_PolyU530/20) and the Theme-Based Research Scheme (T24-504/17-N).

References

Aiken, A. C., DeCarlo, P. F., Kroll, J. H., Worsnop, D. R., Huffman, J. A., Docherty, K. S., Ulbrich, I. M., Mohr, C., Kimmel, J. R., Sueper, D., Sun, Y., Zhang, Q., Trimborn, A., Northway, M., Ziemann, P. J., Canagaratna, M. R., Onasch, T. B., Alfarra, M. R., Prevot, A. S. H., Dommen, J., Duplissy, J., Metzger, A., Baltensperger, U., and Jimenez, J. L.: O/C and OM/OC ratios of primary, secondary, and ambient organic aerosols with High-Resolution Time-of-Flight Aerosol Mass Spectrometry, Environ. Sci. Technol., 42, 4478–4485, doi: 10.1021/es703009q, 2008.

Al-Naiema, I. M. and Stone, E. A.: Evaluation of anthropogenic secondary organic aerosol tracers from aromatic hydrocarbons, Atmos. Chem. Phys., 17, 3, 2053-2065, doi: org/10.5194/acp-17-2053-2017, 2017.

Brege, M., Paglione, M., Gilardoni, S., Decesari, S., Facchini, M. C. and Mazzoleni, L. R.: Molecular insights on aging and aqueous-phase processing from ambient biomass burning emissions-influenced Po Valley fog and aerosol, Atmos. Chem. Phys., 18(17), 13197-13214, doi: org/10.5194/acp-18-13197-2018, 2018.

Canagaratna, M. R., Jayne, J. T., Jimenez, J. L., Allan, J. D., Alfarra, M. R., Zhang, Q., Onasch, T. B., Drewnick, F., Coe, H., Middlebrook, A., Delia, A., Williams, L. R., Trimborn, A. M., Northway, M. J., DeCarlo, P. F., Kolb, C. E., Davidovits, P., and Worsnop, D. R.: Chemical and microphysical characterization of ambient aerosols with the aerodyne aerosol mass spectrometer, Mass Spectrom. Rev., 26, 185-222, doi: 10.1002/mas.20115, 2007.

Canagaratna, M. R., Jimenez, J. L., Kroll, J. H., Chen, Q., Kessler, S. H., Massoli, P., Hildebrandt Ruiz, L., Fortner, E., Williams, L. R., Wilson, K. R., Surratt, J. D., Donahue, N. M., Jayne, J. T., and Worsnop, D. R.: Elemental ratio measurements of organic compounds using aerosol mass spectrometry: characterization, improved calibration, and implications, Atmos. Chem. Phys., 15, 253- 272, doi:10.5194/acp-15-253-2015, 2015.

Clapp, L. J., and Jenkin, M. E.: Analysis of the relationship between ambient levels of O_3, NO_2 and NO as a function of NO_x in the UK, Atmos. Environ., 35, 6391-6405, doi: org/10.1016/S1352-2310(01)00378-8, 2001.

DeCarlo, P. F., Kimmel, J. R., Trimborn, A., Northway, M. J., Jayne, J. T., Aiken, A. C., Gonin, M., Fuhrer, K., Horvath, T., Docherty, K. S., Worsnop, D. R., and Jimenez, J. L.: Field-deployable, high-resolution, time-of-flight aerosol mass spectrometer, Anal. Chem., 78, 8281-8289, doi: 10.1021/ac061249n, 2006.

DeCarlo, P. F., Ulbrich, I. M., Crounse, J., Foy, B., Dunlea, E. J., Aiken, A. C., Knapp, D., Weinheimer, A. J., Campos, T., Wennberg, P. O., and Jimenez, J. L.: Investigation of the sources and processing of organic aerosol over the Central Mexican Plateau from aircraft measurements during MILAGRO, Atmos. Chem. Phys., 10,12, 5257-5280, doi: org/10.5194/acp-10-5257-2010, 2010.

De Gouw, J. and Jimenez, J. L.: Organic aerosols in the Earth's atmosphere, Environ. Sci. Technol., 43, 7614–7618, doi: 10.1021/es9006004, 2009.

Donahue, N. M., Robinson, A. L., Stanier, C. O. and Pandis, S. N.: Coupled partitioning, dilution, and chemical aging of semivolatile organics, Environ. Sci. Technol., 40, 8, 2635-2643, doi: org/10.1021/es052297c, 2006.

Elser, M., Huang, R. J., Wolf, R., Slowik, J. G., Wang, Q., Canonaco, F., and Prévôt, A. S.: New insights into $PM_{2.5}$ chemical composition and sources in two major cities in China during extreme haze events using aerosol mass spectrometry, Atmos. Chem. Phys., 16(5), 3207-3225, 2016.

Friese, E. and Ebel, A.: Temperature dependent thermodynamic model of the system $H^+ - NH_4^+ - Na^+ - SO_4^{2-} - NO_3^- - Cl^- - H_2O$, J. Phys. Chem. A, 114(43), 11595-11631, 2010.

He, L. Y., Huang, X. F., Xue, L., Hu, M., Lin, Y., Zheng, J., Zhang, R. Y. and Zhang, Y. H.: Submicron aerosol analysis and organic source apportionment in an urban atmosphere in Pearl River Delta of China using high-resolution aerosol mass spectrometry, J. Geophys. Res., 116, doi: org/10.1029/2010JD014566, 2011.

Hu, D., and Yu, J. Z.: Secondary organic aerosol tracers and malic acid in Hong Kong: seasonal trends and origins, Environ. Chem., 10, 5, 381-394, doi:org/10.1071/EN13104, 2013.

Hu, W., Hu, M., Hu, W. W., Zheng, J., Chen, C., Wu, Y., and Guo, S.: Seasonal variations in high time-resolved chemical compositions, sources, and evolution of atmospheric submicron aerosols in the megacity Beijing, Atmos. Chem. Phys., 17, 9979-10000, doi: 10.5194/acp-17-9979-2017, 2017.

Huang, D. D., Kong, L., Gao, J., Lou, S., Qiao, L., Zhou, M., and Huang, C.: Insights into the formation and properties of secondary organic aerosol at a background site in Yangtze River Delta region of China: Aqueous-phase processing vs. photochemical oxidation, Atmos. Environ., 239, 117716, doi: org/10.1016/j.atmosenv.2020.117716, 2020.

Huang, R., Zhang, Y., Bozzetti, C. et al: High secondary aerosol contribution to particulate pollution during haze events in China, Nature, 514, 218–222, doi: org/10.1038/nature13774, 2014.

Jacob, D. J. and Winner, D. A.: Effect of climate change on air quality, Atmos. Environ., 43(1), 51-63, doi: org/10.1016/j.atmosenv.2008.09.051, 2009.

Jayne, J. T., Leard, D. C., Zhang, X. F., Davidovits, P., Smith, K. A., Kolb, C. E., and Worsnop, D. R.: Development of an aerosol mass spectrometer for size and composition analysis of submicron particles, Aerosol Sci. Tech., 33, 49-70, doi: 10.1080/027868200410840, 2000.

Jimenez, J. L., Jayne, J. T., Shi, Q., Kolb, C. E., Worsnop, D. R., Yourshaw, I., Seinfeld, J. H., Flagan, R. C., Zhang, X., Smith, K. A., Morris, J. W., and Davidovits, P.: Ambient aerosol sampling with an Aerosol Mass Spectrometer, J. Geophys. Res.-Atmos., 108, 8425, doi:8410:1029/2001JD001213, 2003.

Jimenez, J. L., Canagaratna, M. R., Donahue, N. M., Prevot, A. S. H., Zhang, Q., Kroll, J. H., DeCarlo, P. F., Allan, J. D., Coe, H., Ng, N. L., Aiken, A. C., Docherty, K. S., Ulbrich, I. M., Grieshop, A. P., Robinson, A. L., Duplissy, J., Smith, J. D., Wilson, K. R., Lanz, V. A., Hueglin, C., Sun, Y. L., Tian, J., Laaksonen, A., Raatikainen, T., Rautiainen, J., Vaattovaara, P., Ehn, M., Kulmala, M., Tomlinson, J. M., Collins, D. R., Cubison, M. J., Dunlea, J., Huffman, J. A., Onasch, T. B., Alfarra, M. R., Williams, P. I., Bower, K., Kondo, Y., Schneider, J., Drewnick, F., Borrmann, S., Weimer, S., Demerjian, K., Salcedo, D., Cottrell, L., Griffin, R., Takami, A., Miyoshi, T., Hatakeyama, S., Shimono, A., Sun, J. Y., Zhang, Y. M., Dzepina, K., Kimmel, J. R., Sueper, D., Jayne, J. T., Herndon, S. C., Trimborn, A. M., Williams, L. R., Wood, E. C., Middlebrook, A. M., Kolb, C. E., Baltensperger, U., and Worsnop, D. R.: Evolution of organic aerosols in the atmosphere, Science, 326, 1525-1529, doi: 10.1126/science.1180353, 2009.

Kanakidou, M., Seinfeld, J. H., Pandis, S. N., Barnes, I., Dentener, F. J., Facchini, M. C. and Wilson, J.: Organic aerosol and global climate modelling: a review, Atmos. Chem. Phys., 5(4), 1053-1123, doi: org/10.5194/acp-5-1053-2005, 2005.

Kim, H., Zhang, Q., Bae, G. N., Kim, J. Y., and Lee, S. B.: Sources and atmospheric processing of winter aerosols in Seoul, Korea: insights from real-time measurements using a high-resolution aerosol mass spectrometer, Atmos. Chem. Phys., 17, 2009-2033, doi:10.5194/acp-17-2009-2017, 2017.

Kroll, J. H. and Seinfeld, J. H.: Chemistry of secondary organic aerosol: Formation and evolution of low-volatility organics in the atmosphere, Atmos. Environ., 42, 16, 3593-3624, doi: org/10.1016/j.atmosenv.2008.01.003, 2008.

Lanz, V. A., Alfarra, M. R., Baltensperger, U., Buchmann, B., Hueglin, C., and Prévôt, A. S. H.: Source apportionment of submicron organic aerosols at an urban site by factor analytical modelling of aerosol mass spectra, Atmos. Chem. Phys., 7, 1503-1522, doi:10.5194/acp-7-1503-2007, 2007.

Lanz, V. A., Alfarra, M. R., Baltensperger, U., Buchmann, B., Hueglin, C., Szidat, S., Wehrli, M. N., Wacker, L., Weimer, S., Caseiro, A., Puxbaum, H., and Prevot, A. S. H.: Source attribution of submicron organic aerosols during wintertime inversions by advanced factor analysis of aerosol mass spectra, Environ. Sci. Technol., 42, 214–220, doi:10.1021/es0707207, 2008.

Lee, B. P., Li, Y. J., Yu, J. Z., Louie, P. K., and Chan, C. K.: Characteristics of submicron particulate matter at the urban roadside in downtown Hong Kong- Overview of 4 months of continuous high-resolution aerosol mass spectrometer measurements, J. Geophys. Res., 120, 7040-7058, doi: 10.1002/2015JD023311, 2015.

Li, Y., Pöschl, U. and Shiraiwa, M.: Molecular corridors and parameterizations of volatility in the chemical evolution of organic aerosols, Atmos. Chem. Phys., 16, 5, doi: org/10.5194/acp-16-3327-2016, 3327-3344, 2016.

Li, Y. J., Lee, B. Y. L., Yu, J. Z., Ng, N. L., and Chan, C. K.: Evaluating the degree of oxygenation of organic aerosol during foggy and hazy days in Hong Kong using high-resolution time-of-flight aerosol mass spectrometry (HR-ToF-AMS), Atmos. Chem. Phys., 13, 8739-8753, doi: 10.5194/acp-13-8739-2013, 2013.

Li, Y. J., Lee, B. P., Su, L., Fung, J. C. H., and Chan, C. K.: Seasonal characteristics of fine particulate matter (PM) based on high-resolution time-of-flight aerosol mass spectrometric (HR-ToF-AMS) measurements at the HKUST Supersite in Hong Kong, Atmos. Chem. Phys., 15, 37-53, doi: 10.5194/acp-15-37-2015, 2015.

Lin, C., Li, Y., Lau, A. K. H., Li, C. C. and Fung, J. C. H.:15-year $PM_{2.5}$ trends in the Pearl River Delta region and Hong Kong from satellite observation, Aerosol Air. Qual. Res., 8, 2355-2362, doi: org/10.4209/aaqr.2017.11.0437, 2018.

Liu, T., Zhou, L., Liu, Q., Lee, B. P., Yao, D., Lu, H., Lyu, X., Guo, H., and Chan, C. K.: Secondary organic aerosol formation from urban roadside air in Hong Kong, Environ. Sci. Technol., 53, 3001-3009, doi: 10.1021/acs.est.8b06587, 2019.

Liu, X., Wang, N., Lyu, X., Zeren, Y., Jiang, F., Wang, X., Zou, S., Ling, Z. and Guo, H.: Photochemistry of ozone pollution in autumn in Pearl River Estuary, South China, Sci. Total Environ., 754, 141812, doi: org/10.1016/j.scitotenv.2020.141812, 2021.

Lyu, X., Guo, H., Yao, D., Lu, H., Huo, Y., Xu, W., Kreisberg, N., Goldstein, A. H., Jayne, J., Worsnop, D., Tan, Y., Lee, S. C. and Wang, T.: In situ measurements of molecular markers facilitate understanding of dynamic sources of atmospheric organic aerosols, Environ. Sci. Technol., 54(18), 11058-11069, doi: org/10.1021/acs.est.0c02277, 2020.

Marshall, J. D., Nethery, E. and Brauer, M.: Within-urban variability in ambient air pollution: comparison of estimation methods, Atmos. Environ., 42, 1359-1369, doi: org/10.1016/j.atmosenv.2007.08.012, 2008.

Ng, N. L., Canagaratna, M. R., Jimenez, J. L., Chhabra, P. S., Seinfeld, J. H., and Worsnop, D. R.: Changes in organic aerosol composition with aging inferred from aerosol mass spectra, Atmos. Chem. Phys., 11, 6465-6474, doi: 10.5194/acp-11-6465-2011, 2011.

570 Paatero, P. and Tapper, U.: Positive matrix factorization- A nonnegative factor model with
571 optimal utilization of error-Estimates of data values, Environmetrics, 5, 111- 126,
572 doi:10.1002/env.3170050203, 1994.

573 Paglione, M., Gilardoni, S., Rinaldi, M., Decesari, S., Zanca, N., Sandrini, S., and Fuzzi, S:
574 The impact of biomass burning and aqueous-phase processing on air quality: a multi-year
575 source apportionment study in the Po Valley, Italy, Atmos. Chem. Phys., 20, 1233-1254, doi:
576 org/10.5194/acp-20-1233-2020, 2020.

577 Qin, Y. M., Li, Y. J., Wang, H., Lee, B. P., Huang, D. D. and Chan, C. K.: Particulate matter
578 (PM) episodes at a suburban site in Hong Kong: evolution of PM characteristics and role of
579 photochemistry in secondary aerosol formation, Atmos. Chem. Phys., 16, 14131-14145, doi:
580 10.5194/acp-16-14131-2016, 2016.

581 Seinfeld, J. and Pandis, S.: Atmospheric Chemistry and Physics, 1997, New York, doi:
582 org/10.12987/9780300150315, 2008.

583 So, K. L., Guo, H. and Li, Y. S.: Long-term variation of $PM_{2.5}$ levels and composition at rural,
584 urban, and roadside sites in Hong Kong: Increasing impact of regional air pollution, Atmos.
585 Environ., 41, 40, 9427-9434, doi: org/10.1016/j.atmosenv.2007.08.053, 2007.

586 Sun, Y. L., Zhang, Q., Schwab, J. J., Demerjian, K. L., Chen, W. N., Bae, M. S., Hung, H. M.,
587 Hogrefe, O., Frank, B., Rattigan, O. V., and Lin, Y. C.: Characterization of the sources and
588 processes of organic and inorganic aerosols in New York city with a high-resolution time-of-
589 flight aerosol mass spectrometer, Atmos. Chem. Phys., 11, 1581–1602, doi:10.5194/acp-11-
590 1581- 2011, 2011.

591 Tan, Y., Han, S., Chen, Y., Zhang, Z., Li, H., Li, W., Yuan, Q., Li, X., Wang, T., and Lee, S.
592 C.: Characteristics and source apportionment of volatile organic compounds (VOCs) at a
593 coastal site in Hong Kong, Sci. Total Environ., 777, 146241, doi:
594 org/10.1016/j.scitotenv.2021.146241, 2021.

595 Ulbrich, I. M., Canagaratna, M. R., Zhang, Q., Worsnop, D. R., and Jimenez, J. L.:
596 Interpretation of organic components from Positive Matrix Factorization of aerosol mass
597 spectrometric data, Atmos. Chem. Phys., 9, 2891-2918, doi:10.5194/acp-9-2891-2009, 2009.

598 Wang, Y., Wang, H., Guo, H., Lyu, X, Cheng, H., Ling, Z., Louie, P.K., Simpson, I.J., Meinardi
599 I.J. and Blake, D.R.: Long-term O_3-precursor relationships in Hong Kong: field observation
600 and model simulation, Atmos. Chem. Phys., 17, 10919-10935, doi: org/10.5194/acp-17-10919-
601 2017, 2017.

602 Wang, T.; Dai, J.; Lam, K. S.; Poon, C. N. and Brasseur, G. P.: Twenty-Five Years of Lower
603 Tropospheric Ozone Observations in Tropical East Asia: The Influence of Emissions and
604 Weather Patterns, Geophys. Res. Lett. 2019, 46 (20), 11463−11470.

Wang, W., Wu, M. H., Li, L., Zhang, T., Li, H. J., Wang, Y. J., Liu, X. D., Sheng, G. Y., Claeys, M. and Fu, J. M.: Polar organic tracers in $PM_{2.5}$ aerosols from forests in eastern China, Atmos. Chem. Phys., 8, 7507. doi:10.5194/ACP-8-7507-2008, 2008.

Wexler, A. S. and Clegg, S. L.: Atmospheric aerosol models for systems including the ions H^+, NH_4^+, Na^+, SO_4^{2-}, NO_3^-, Cl^-, Br^-, and H_2O, J. Geophys. Res., 107(D14), ACH-14, 2002.

Xiao, Y., Hu, M., Zong, T., Wu, Z., Tan, T., Zhang, Z., Fang, X., Chen, S., and Guo, S.: Insights into aqueous-phase and photochemical formation of secondary organic aerosol in the winter of Beijing, Atmos. Environ., 118535. doi: org/10.1016/j.atmosenv.2021.118535, 2021.

Xu, L., Guo, H., Boyd, C. M., Klein, M., Bougiatioti, A., Cerully, K. M., Hite, J. R., Isaacman-VanWertz, G., Kreisberg, N. M., Knote, C., Olson, K., Koss, A., Goldstein A. H., Hering, S. V., Gouw, J., Baumann, K., Lee, S. H., Nenes, A., Weber, R. J. and Ng, N. L.: Effects of anthropogenic emissions on aerosol formation from isoprene and monoterpenes in the southeastern United States, Proc. Natl. Acad. Sci., 112, 1, 37-42, doi: 10.1073/pnas.1512277112, 2015.

Xu, W., Han, T., Du, W., Wang, Q., Chen, C., Zhao, J., Zhang, Y., Li, J., Fu, P., Wang, Z., Worsnop, D.R., and Sun, Y.: Effects of aqueous-phase and photochemical processing on secondary organic aerosol formation and evolution in Beijing, China, Environ. Sci. Technol., 51(2), 762-770, doi: org/10.1021/acs.est.6b04498, 2017.

Zhang, Q., Alfarra, M. R., Worsnop, D. R., Allan, J. D., Coe, H., Canagaratna, M. R., and Jimenez, J. L.: Deconvolution and quantification of hydrocarbon-like and oxygenated organic aerosols based on aerosol mass spectrometry, Environ. Sci. Technol., 39, 4938–4952, doi:10.1021/es048568l, 2005.

Zhang, Q., Jimenez, J. L., Canagaratna, M. R., Ulbrich, I. M., Ng, N. L., Worsnop, D. R., and Sun, Y.: Understanding atmospheric organic aerosols via factor analysis of aerosol mass spectrometry: a review, Anal. Bioanal. Chem., 401, 3045–3067, doi: 10.1007/s00216-011-5355-y, 2011.

Zhang, Y. N.; Zhang, Z. S.; Chan, C. Y.; Engling, G.; Sang, X. F.; Shi, S., and Wang, X. M.: Levoglucosan and carbonaceous species in the background aerosol of coastal southeast China: case study on transport of biomass burning smoke from the Philippines, Environ. Sci. Pollut. Res. 2012, 19 (1), 244−255.

Zhou, L., Liu, T., Yao, D., Guo, H., Cheng, C. and Chan, C. K.: Primary emissions and secondary production of organic aerosols from heated animal fats, Sci. Total Environ., 148638, doi: org/10.1016/j.scitotenv.2021.148638, 2021.